Available online at www.sciencedirect.com
ScienceDirect
Developmental Biology 306 (2007) 525–537
DEVELOPMENTAL BIOLOGY
www.elsevier.com/locate/ydbio

Altering the speract-induced ion permeability changes that generate flagellar Ca^{2+} spikes regulates their kinetics and sea urchin sperm motility

Christopher D. Wood [a,*], Takuya Nishigaki [a], Yoshiro Tatsu [b], Noboru Yumoto [b], Shoji A. Baba [c], Michael Whitaker [d], Alberto Darszon [a]

[a] *Departamento de Genética del Desarrollo y Fisiología Molecular, Instituto de Biotecnología, Universidad Nacional Autónoma de México, UNAM, Apdo Postal 510-3, Cuernavaca, Morelos 62250, México*
[b] *National Institute of Advanced Industrial Science and Technology (AIST), Midorigaoka, Ikeda 563-8577, Japan*
[c] *Department of Biology, Ochanomizu University, Tokyo 112-8610, Japan*
[d] *Institute of Cell and Molecular Biosciences, Faculty of Medical Sciences, University of Newcastle, Newcastle upon Tyne, UK*

Received for publication 15 November 2006; revised 22 March 2007; accepted 22 March 2007
Available online 30 March 2007

Abstract

Speract, an egg-derived sperm-activating peptide, induces changes in intracellular Ca^{2+}, Na^{+}, pH, cAMP, cGMP, and membrane potential in sperm of the sea urchin *Strongylocentrotus purpuratus*. Ca^{2+} is a key regulator of motility in all sperm and, in many marine species, is required for generating turns interspersed with straighter swimming paths that are essential for chemotaxis towards the egg. We show that speract triggers a train of increases in flagellar Ca^{2+}, and that each individual Ca^{2+} fluctuation induces a transient increase in flagellar asymmetry that leads to a turn. We also find that modifying the amplitude, duration and interval between individual Ca^{2+} fluctuations by treating sperm with niflumic acid, an inhibitor of Ca^{2+}-activated Cl^{-} channels, correspondingly alters the properties of the sperm turns. We conclude that Ca^{2+} entry through a fast flagellar pathway not only induces sperm turns, but the kinetics of Ca^{2+} entry may shape the nature of these turns, and that these kinetics are tuned by other channels, possibly including Cl^{-} channels. In addition, the speract-induced changes in sperm motility closely resemble those seen during chemotaxis in other marine organisms, yet speract is not a chemoattractant. This implies the Ca^{2+}-induced motility changes are necessary but not sufficient for chemotaxis.

Keywords: Calcium; Sea urchin; Sperm; Motility; Flagella

Introduction

Sperm from a diverse range of organisms, from bracken ferns, many marine species and mammals, follow chemical cues in their journey to locate and fertilise the egg or oocyte, called chemotaxis (Brokaw, 1974; Eisenbach and Giojalas, 2006; Kaupp et al., 2006; Miller et al., 1985). In sea urchins, short peptides (sperm activating peptides, or SAPs) diffuse away from the outer egg investments to activate sperm metabolism and modify sperm motility (Cook et al., 1994; Shiba et al., 2005). Sea urchin sperm are a useful model for studying flagellar-driven motility, as the sperm swim with a plane circular trajectory of ~50 μm diameter for extended periods when confined in an imaging chamber. This is due to their flagella beating in near-planar waves that are displaced to one side in relation to the long axis of the head (Cosson et al., 2003) that in natural conditions generate a helical trajectory. In the presence of SAPs, sea urchin sperm undergo a series of transient turns interspersed with periods of straighter swimming that together direct the sperm to swim towards the egg (Kaupp et al., 2003; Ward et al., 1985). Sperm turns are the product of transient increases in flagellar asymmetry (Miller and Brokaw, 1970). The generation of turns is central to chemotaxis, as under conditions whereby the transient increases in flagellar asymmetry are inhibited, for example in the absence of external Ca^{2+}, chemotaxis fails to occur (Brokaw, 1974; Cosson et al., 1984; Spehr et al., 2003; Ward et al., 1985).

* Corresponding author. Fax: +52 777 3172388.
E-mail address: chris@ibt.unam.mx (C.D. Wood).

0012-1606/$ - see front matter © 2007 Elsevier Inc. All rights reserved.
doi:10.1016/j.ydbio.2007.03.036

SAPs bind to flagellar receptors to stimulate a variety of downstream signalling pathways (Darszon et al., 2001). This pathway remains to be definitively characterised, but most work has been performed using speract, a decapeptide SAP isolated from the egg investments of *Strongylocentrotus purpuratus*. Binding of speract to its receptor in the flagellum (Cardullo et al., 1994; Dangott and Garbers, 1984) rapidly activates a guanylate cyclase (Ramarao and Garbers, 1985) that leads to an increase in cGMP (Cook and Babcock, 1993b; Hansbrough and Garbers, 1981; Harumi et al., 1992). There then follows a hyperpolarisation, probably through opening of K^+ channels (Babcock et al., 1992; Lee and Garbers, 1986), that have been proposed to be directly activated by cGMP (Galindo et al., 2000, 2007), as has been shown in a different sea urchin, *Arbacia punctulata* (Strunker et al., 2006). The hyperpolarisation activates an increase in intracellular pH (pH_i) (Babcock et al., 1992; Lee and Garbers, 1986; Reynaud et al., 1993; Schackmann and Chock, 1986), a transient $[Ca^{2+}]_i$ decrease (Nishigaki et al., 2004), and has been suggested to remove inactivation from voltage-gated Ca^{2+} (Cav) channels (Granados-Gonzalez et al., 2005; Strunker et al., 2006) which can then open as a consequence of a depolarisation, such as the speract-induced repolarisation (Darszon et al., 2005). Increases in cAMP and intracellular Na^+ also follow the hyperpolarisation (Garbers, 1989; Rodriguez and Darszon, 2003).

The key role of Ca^{2+} ions in regulating sperm chemotaxis is long-established, being an essential requirement for all sperm chemotactic mechanisms identified thus far. Uncaging of cGMP in motile *S. purpuratus* and *A. punctulata* sperm induced turns followed by periods of straighter swimming (Bohmer et al., 2005; Kaupp et al., 2003; Wood et al., 2005), the swimming pattern characteristically seen during chemotaxis. External Ca^{2+} is essential for generating these cGMP-induced turns, and in the case of *S. purpuratus* sperm, Ca^{2+} entry through a specific, rapidly activated, flagellar pathway is necessary; Ca^{2+} entry through one or more secondary pathways did not induce the sperm to turn (Wood et al., 2005). Inhibitors of Ca_v channels selectively inhibited this rapid flagellar pathway and also blocked sperm turning, and Ca_v channel antibodies stain the flagella of *S. purpuratus* sperm (Granados-Gonzalez et al., 2005). A partial sequence of a T-type Ca_v channel has also been found in the *S. purpuratus* genome (Strunker et al., 2006). Nevertheless, it remains possible that the uncaging of cGMP does not reproduce the precise characteristics of intracellular changes in cGMP (compartmentalisation, kinetics, overall concentration, etc.) that occur following speract binding. Indeed, in single immobilised cells, speract induces a train of fluctuations in $[Ca^{2+}]_i$ (Wood et al., 2003) that were not observed following uncaging of cGMP in motile cells (Wood et al., 2005). Here we use caged speract to stimulate motile *S. purpuratus* sperm and record changes in $[Ca^{2+}]_i$ in their flagella, and investigate the relationship between increases in $[Ca^{2+}]_i$ and flagellar motility. We also modified the amplitude, duration and periodicity of the Ca^{2+} fluctuations by treating cells with niflumic acid, an anion channel inhibitor, and propose a model for the generation of Ca^{2+} fluctuations in the flagella of sea urchin sperm based on these results.

Materials and methods

Materials

Sperm were obtained 'dry' from *S. purpuratus* (Marinus Inc., Long Beach, CA, USA; Pamanes S. A. de C.V., Ensenada, Mexico) by intercoelomic injection of 0.5 M KCl and stored on ice. Artificial sea water (ASW), zero Ca^{2+} ASW, and high K^+ ASW prepared as described (Wood et al., 2003). [Ser^5; nitrobenzyl-Gly^6]speract (and referred to throughout the text as 'caged speract') was prepared as previously described (Tatsu et al., 2002). Fluo-4-AM, BCECF-AM and $DiSC_3(5)$ and pluronic F-127 were from Molecular Probes, Inc. (Eugene, OR, USA). Nimodipine was from Tocris Cookson Inc. (Ellisville, MO, USA). PolyHEMA (poly(2-hydroxyethyl methacrylate)), Triton X-100, SK&F 96365, oligomycin, valinomycin, niflumic acid and tributyltin were from Sigma-Aldrich Quimica S.A. de C.V. (Toluca, Edo de Mexico, Mexico).

Loading of fluorescent indicators

Sperm for single-cell motility analyses were prepared as previously described (Wood et al., 2005). Sperm measured in the spectrophotometer were prepared as described in Nishigaki et al. (2004).

Fluorescence imaging of swimming sperm

All coverslips were prepared and imaging chambers assembled and mounted as previously indicated (Wood et al., 2005). Epifluorescence images were collected with either a Nikon Plan Apo 60× 1.4NA or a Nikon Plan Fluor 40× 1.3NA objective using a Chroma filter set (ex, HQ470/40×; DC, 505DCXRU; em, HQ510LP) and recorded on a Quantix 57 CCD camera (Photometrics Inc., Tucson, AZ, USA). Fluorescence illumination was supplied by a Luxeon V Star Lambertian Cyan LED part # LXHL-LE5C (Lumileds Lighting LLC, San Jose, USA) attached to a custom-built stroboscopic control box. The LED was mounted into a FlashCube40 assembly with dichroic mirror M40-DC400 (Rapp Opto Electronic, Hamburg). LED output was synchronized to the Exposure Out signal of the Quantix 57 camera via the control box to produce a single flash of 2 ms duration per individual exposure. The camera exposure time was set equivalent to flash duration (2 ms). Images were collected every ~25 ms with exposure time during duty cycle of 8%. Images were collected with iQ software (Andor Bioimaging, NC). Photolysis of caged speract was via a 100 W mercury lamp filtered through a UV band-pass filter (270–400 nm) connected to the FlashCube40 side-port with a Uniblitz VS35S2ZM1R1-27 shutter (Vincent Associates, NY) and triggered by BoB unit (Andor Bioimaging, NC) connected to a Master 8 pulse generator (A.M.P.I., Jerusalem, Israel).

Determination of sperm $[Cl^-]_i$

Determination of sperm $[Cl^-]_i$ was performed by the null point method (adapted from Babcock, 1983). To measure $[Cl^-]_i$, tributyltin (10 μM), a Cl^-/OH^- exchanger, was used in combination with the pH indicator BCECF (ex 500 nm, em 540 nm) in an Aminco SLM 8000 spectrofluorometer (SLM Instruments, IL) using 800 μl of sperm suspension with magnetic stirring at 15 °C (Nishigaki et al., 2004). At the null point the ionophore does not alter pH_i when the combined H^+ and Cl^- gradients are equilibrated between the cytoplasm and the medium. To vary the $[Cl^-]_e$, seawater containing 20 mM Cl^- was mixed with ASW at varying ratios. The ionic composition of low Cl^- ASW was (mM): 515 Na gluconate, 10 $CaCl_2$, 50 $MgSO_4$, 10 KOH, 2.5 $NaHCO_3$, 10 HEPES (pH 6.8–7.2, 1000 mosM). ASW contained (mM): 486 NaCl, 10 $CaCl_2$, 10 KCl, 27 $MgCl_2$, 29 $MgSO_4$, 2.5 $NaHCO_3$, 0.1 EDTA and 10 HEPES (pH 6.8–7.2, 1000 mOsm). Before each experiment 0.025 % Triton X-100 was added to a BCECF-loaded sperm sample and the pH of the sea water adjusted to eliminate any large change in fluorescence upon release of BCECF.

Membrane potential (E_m) measurements

Sperm E_m was measured in the spectrofluorometer with $DiSC_3(5)$ (ex 620 nm, em 670 nm). About 5 μl of 10-fold diluted sperm were suspended in 800 μl of ASW (pH 8.0) with 200 nM of $DiSC_3(5)$ and 1 μM of oligomycin.

After 3–5 min, varying concentrations of niflumic acid (in DMSO; maximum 0.2% v/v) were supplemented, and 2–3 min later, 100 nM speract was added. To calibrate the sperm E_m, 1 μM of valinomycin was added to fix the sperm E_m at the K^+ equilibrium potential (E_K) and followed by stepwise addition of 2 M KCl to a final concentration of 20, 40, and 80 mM K^+. Results are presented as ΔE_m values following speract addition (measured against calibrated scale).

Image processing

Sperm head trajectories, sperm velocities and sperm trajectory curvature were measured using BohBoh software (BohBohSoft, Tokyo, Japan) utilizing an *n*-span (smoothing value) of 4 (Baba and Mogami, 1985). Flagella curvature and fluorescence were measured using the Autotrace module of BohBoh software (*n*-span=7). The change in $[Ca^{2+}]_i$ in the flagellum is stated as fluorescence intensity (FI) representing the average increase in intensity per pixel (12-bit scale) along the length of the flagellum after subtraction of a rolling background value. Due to the inability to measure basal $[Ca^{2+}]_i$ in flagella, these values are an underestimation of the true relative increase of $[Ca^{2+}]_i$ occurring in the flagella. From sampling a random subset of our data the standard deviation of the background noise was between 1.95 and 2.1 counts per pixel. Taking an S.D. of noise of 2 counts per pixel as reference, the signal-to-noise ratio (SNR) of the speract-treated sperm (average value per pixel along flagellum, peak value over course of experiment) ranged from 1.7 to 4.5, and for niflumic acid-treated sperm (5, 10 or 20 μM) the SNR was in the range 5.5–10.3.

Peak and statistical analyses

Peak analyses performed using IgorPro (Wavemetrics, Inc., USA). Peaks in the flagellar Ca^{2+} traces were sequentially and automatically identified using operator-specified peak identification parameters that were uniformly applied to all samples. Each peak was then checked manually and adjustments made to the peak-defining variables if required. Peaks in the curvature traces were then separately and automatically identified by the same method. The two sets of peak information were then exported to Excel and compared side-by-side. Comparing the time post-flash for peaks in the Ca^{2+} and curvature data sets, peaks were considered correlated if a peak in the curvature occurred within ±100 ms of a peak in the Ca^{2+} data set (average interval between Ca^{2+} peaks for cells treated with speract alone=625 ms; minimum interval between Ca^{2+} peaks=200 ms (1 occasion); delay between Ca^{2+} and curvature peak=+26± 6 ms (mean), +25 ms (median), +25 ms (mode)). Any curvature peaks that were identified without a corresponding Ca^{2+} peak were discarded from the analysis. Data are presented from sperm collected from a minimum of three sea urchins. Pearson correlation, Spearman correlation and 1-way ANOVA analyses performed with Analyse-It statistical software (Analyse-it Software, UK), statistical significance derived from all-pairwise multiple comparisons test with Dunnett's and LSD test (two-tailed) with speract-only condition as control. Statistical significance at 95% confidence interval, unless otherwise stated in text.

Results

Effect of uncaging speract on motile S. purpuratus sperm

A caged version of the SAP speract that carries a photocleavable 2-nitrobenzyl group incorporated into the peptide backbone, has a receptor binding affinity approximately 1400× lower than native speract (caged speract IC_{50}=950 nM vs. 0.66 nM for native speract) (Tatsu et al., 2002). Upon exposure to UV, the nitrobenzyl group is rapidly cleaved ($\tau_{1/2}$= 26 μs) to release the decaged adduct (IC50 0.67 nM). *S. purpuratus* sperm loaded with fluo-4 were placed into chambers filled with artificial sea water (ASW) containing 100 nM of caged speract and individual sperm located in the microscope field. Under stroboscopic illumination from a light-emitting diode (LED), only the fluorescent signal from the head could be recorded in unstimulated sperm, as found previously (Wood et al., 2005). Following uncaging of speract by a 250-ms pulse of UV light, $[Ca^{2+}]_i$ increased rapidly and transiently in the sperm flagella, followed by further transient increases in flagellar $[Ca^{2+}]_i$ (Fig. 1; Movie 1 in supplementary material). We then calculated the curvatures of the trajectories of the sperm and observed that sperm could be divided into two populations. Of the 66 sperm analysed, 42 responded to uncaging of speract as shown in Fig. 1A. The motility response in such sperm was biphasic with sharp increases in the curvature of the trajectory (corresponding to turning events) superimposed on a longer, tonic decrease in curvature. In the example in Fig. 1A, each turning event corresponded temporally with individual spikes in flagellar $[Ca^{2+}]_i$. The tonic decrease in curvature corresponded with, and is probably due to, a small reproducible increase in sperm velocity, as reported previously (Bohmer et al., 2005). The trajectory of the sperm is shown in the bottommost panel. The period in which the Ca^{2+} fluctuations occurred is shown in red, and corresponds to the phase in which the sperm traversed from one side of the imaging field to the other. In the periods outside of the Ca^{2+} fluctuations (black traces), little lateral repositioning of the sperm's circular swimming trajectory is observed.

The motility response of the second population (12 of 66 sperm, with a further 11 sperm showing an intermediate response between the two populations) is illustrated in Fig. 1B, in which speract again induces a train of increases in flagellar $[Ca^{2+}]_i$, which also corresponded temporally with individual sperm turns. However in these cells, the tonic phase of the motility response was reversed, in that sperm swam in circles of decreased diameter. This tonic increase in curvature was, as expected, accompanied by a decrease in sperm swimming velocity. The sperm trajectory shown at the bottom of Fig. 1B is typical, in that sperm from this second population do not show large lateral relocations during the Ca^{2+} fluctuation phase (red line).

On one occasion we observed a sperm cross from the first population to the second some seconds after uncaging speract (Fig. 2). In this case, the sperm initiated a sequence of fluctuations in Ca^{2+}, with accompanying turns, superimposed on an underlying tonic decrease in curvature. Just less than 5 s after receiving the UV flash the sperm switched to an underlying increase in curvature, which coincided with a sharp decrease in velocity, whilst the Ca^{2+} fluctuations continued as before. Thus it appears that the two phases of motility change, transient and tonic, are regulated through separate mechanisms, of which only the transient phase appears to depend on increases in flagellar $[Ca^{2+}]_i$. As shown on the bottommost trace, only during the phase of underlying decreased curvature did the sperm display large lateral translocations across the coverslip (red line).

In a previous study, opening of a fast Ca^{2+} entry pathway in flagella following uncaging of cGMP was found to be necessary to generate of sperm turns (Wood et al., 2005), and that this pathway could be inhibited by nimodipine and Ni^{2+}, two agents

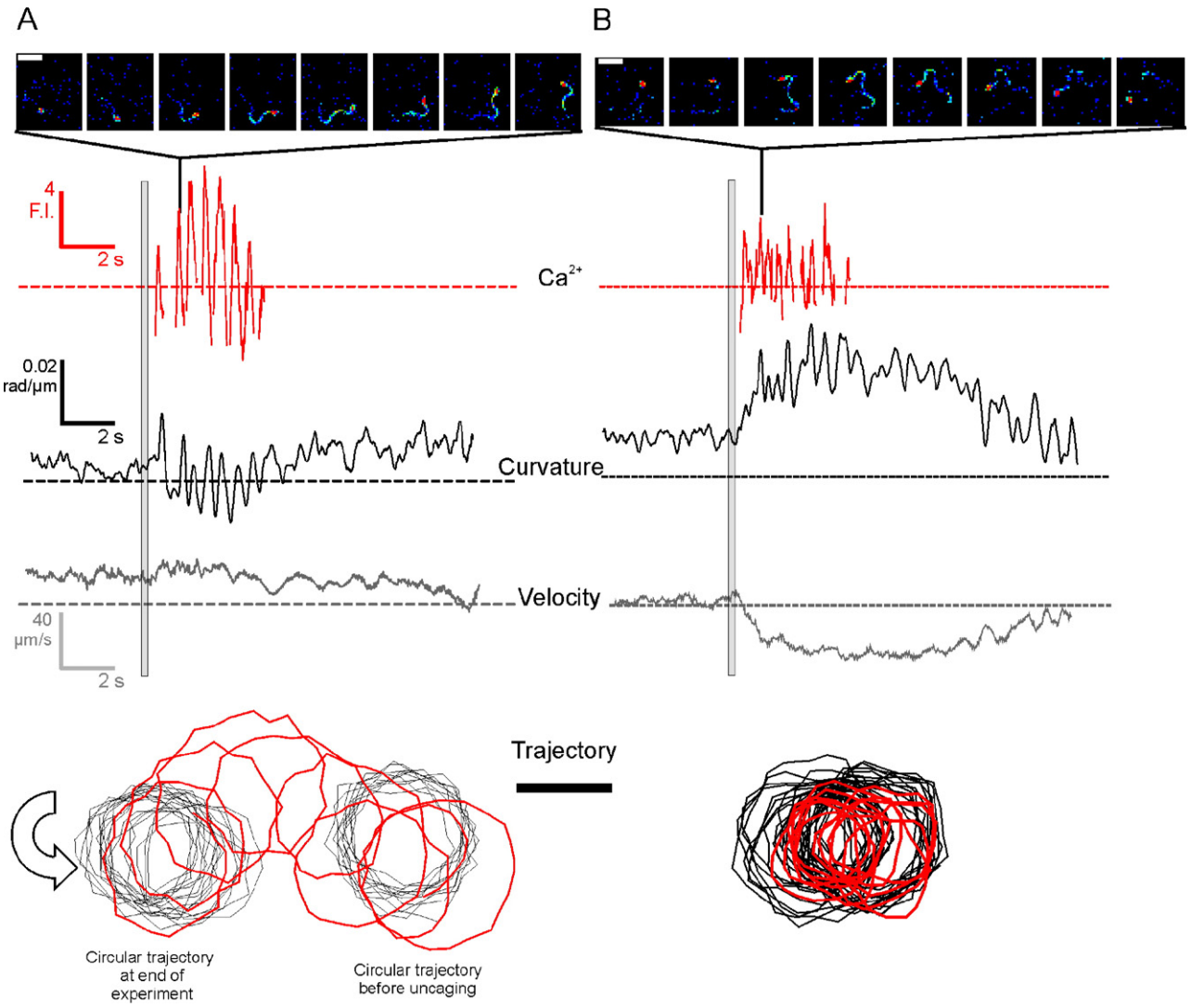

Fig. 1. Speract induces repetitive Ca^{2+} fluctuations in two populations of sperm. (A) Upper panels show images of a typical fast transient increase in fluo-4 fluorescence in the flagella of a motile sperm, extracted from a larger sequence. Interval between successive images=25 ms. Scale bar=20 µm. Red trace shows the fluo-4 fluorescence (average along length) in the flagellum of sperm shown above over complete experiment (18 s); dashed line shows fluorescence intensity (FI) of 4. Black trace shows curvature of sperm trajectory as derived from the position of the head in each frame, dashed line shows curvature of 0.05 rad/µm. Grey trace shows sperm velocity, dashed line shows velocity of 200 µm/s. Grey box indicates UV exposure (250 ms). Bottommost trace shows the sperm swimming trajectory throughout the experiment. The red line is the sperm trajectory during the phase of Ca^{2+} fluctuations, and black lines are the sperm trajectory outside the phase of Ca^{2+} fluctuations. Arrow indicates direction of circular swimming pathway. Scale bar=20 µm. (B) Upper panels show images of a typical fast transient increase in fluo-4 fluorescence in the flagella of a motile sperm from a population that shows a sustained tonic increase in swimming trajectory curvature. All dimensions, intervals and traces as in panel A. Bottommost trace shows the sperm swimming trajectory throughout the experiment. The red line is the sperm trajectory during the phase of Ca^{2+} fluctuations, and black lines are the sperm trajectory outside the phase of Ca^{2+} fluctuations. Arrow indicates direction of circular swimming pathway. Scale bar=20 µm.

that block Ca_v channels. We found that the turning events stimulated by caged speract could also be blocked by these two treatments (effect of Ni^{2+} shown in Figs. 3B, C), and furthermore that in sperm treated with 200 µM Cd^{2+}, an L-type Ca_v channel inhibitor, or 5 µM SK&F 96365, an inhibitor of store-operated Ca^{2+} entry, the turning events were not affected (Figs. 3D, E). We also confirmed that sperm turning events are inhibited in the presence of high external $[K^+]$, and in the absence of external Ca^{2+} (Figs. 3F, G), although in this latter condition, the tonic decrease in the curvature of the trajectory was unaffected, as reported previously (Bohmer et al., 2005; Kaupp et al., 2003; Wood et al., 2005).

Flagellar Ca^{2+} increases do not always result in an increase in flagellar asymmetry

We next looked at the effect of decreasing the concentration of caged speract in the extracellular medium. At 0.1 nM caged speract we observed no increase in $[Ca^{2+}]_i$ nor motility changes, even if the exposure time to UV light was increased to 0.5 s (data not shown). At 1 nM caged speract approximately half (n=12) of the sperm tested showed a response after a 250-ms exposure to UV light. At this concentration, the delay to the first Ca^{2+} elevation increased on average from 225±50 ms (n=13) to 1300±550 ms (n=5),

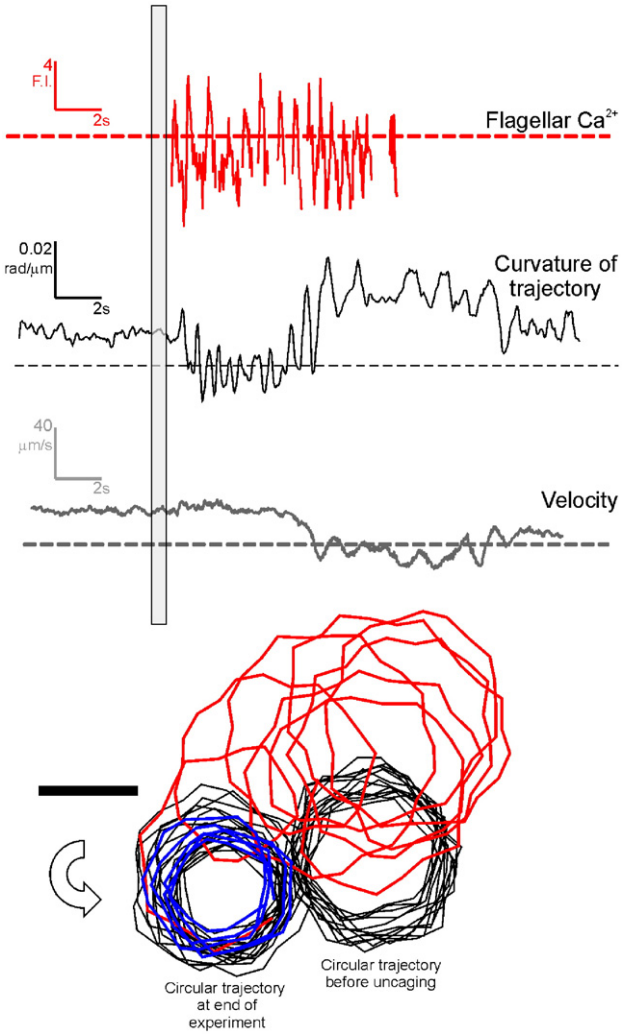

Fig. 2. Sperm may rapidly switch from decrease to an increase in the underlying tonic curvature of the swimming trajectory. Red trace shows the fluo-4 fluorescence (average along length) of flagellum, dashed line indicates a fluorescence intensity of 5. Black trace shows curvature of sperm trajectory as derived from the position of the head in each frame, dashed line denotes a curvature of 0.05 rad/µm. Grey trace shows sperm velocity, dashed line represents a velocity of 200 µm/s. Grey box indicates UV exposure (250 ms). Bottommost trace shows the sperm swimming trajectory throughout the experiment. The red line is the sperm trajectory during the phase of Ca^{2+} fluctuations and underlying decreased curvature. The blue line is the sperm trajectory during the phase of Ca^{2+} fluctuations and underlying increased curvature. Black lines are the sperm trajectory outside the phase of Ca^{2+} fluctuations. Scale bar=20 µm.

and in two sperm, a small transient increase in flagellar Ca^{2+} preceded a larger increase in $[Ca^{2+}]_i$ (Fig. 4; Movie 2 in supplementary materials). Notably, the smaller initial increase in Ca^{2+} did not increase flagellar asymmetry nor cause the sperm to turn, in contrast to the subsequent larger increase in $[Ca^{2+}]_i$.

Niflumic acid increases the amplitude, duration and interval between successive fluctuations in flagellar $[Ca^{2+}]_i$

In experiments in immobilised *S. purpuratus* sperm, niflumic acid [commonly used as an inhibitor of Ca^{2+}-activated Cl^- channels (CaCC) (e.g. Pacaud et al., 1989)] dramatically altered the nature of the fluctuations in $[Ca^{2+}]_i$ (Wood et al., 2003). In the presence of niflumic acid, the speract-induced fluctuations increased in both amplitude and duration, and the interval between successive fluctuations was both larger and more periodic. We decided to investigate whether niflumic acid had the same effect on $[Ca^{2+}]_i$ increases in motile cells, and if so, how these changes influence flagellar form and sperm motility.

Fig. 5A shows the effect, following release of caged speract, of 10 µM niflumic acid on swimming sperm. As in immobilised sperm, niflumic acid increased the amplitude and duration of Ca^{2+} increases in the flagella, and increased the interval between successive individual transient Ca^{2+} fluctuations (see also Movie 3 in supplementary material). Fig. 5B contains images that partially span individual Ca^{2+} fluctuations from sperm treated with 100 nM caged speract alone (upper panels)

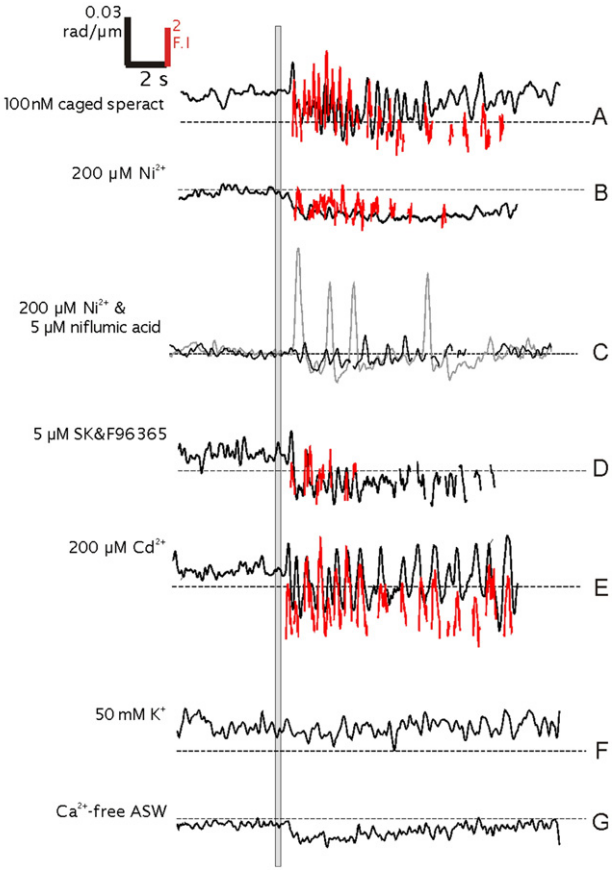

Fig. 3. Head trajectory curvatures and $[Ca^{2+}]_i$ of sperm treated with various pharmacological agents and extracellular media. (A) Curvature of sperm trajectory (black line) and $[Ca^{2+}]_i$ fluctuations (red line) in sperm exposed to 100 nM caged speract and 250 ms UV light (grey box). (B) As in panel A, but in the additional presence of 200 µM Ni^{2+}. (C) Black line shows curvature of sperm trajectory after exposure to 250 ms UV in the presence of 100 nM caged speract, 200 µM Ni^{2+} and 5 µM niflumic acid. Grey line shows effect of omitting Ni^{2+}. (D) As in panel A, but in the additional presence of SK and F96365. (E) As in panel A, but in the additional presence of 200 µM Cd^{2+}. (F) Raising $[K^+]_e$ to 50 mM inhibits motility response of sperm exposed to 250 ms UV and 100 nM caged speract. (G) Removing external Ca^{2+} inhibits the turning events, but not the tonic decrease in curvature, following exposure to 250 ms UV in 100 nM caged speract. In all traces, the dashed line indicates a curvature of 0.05 rad/µm.

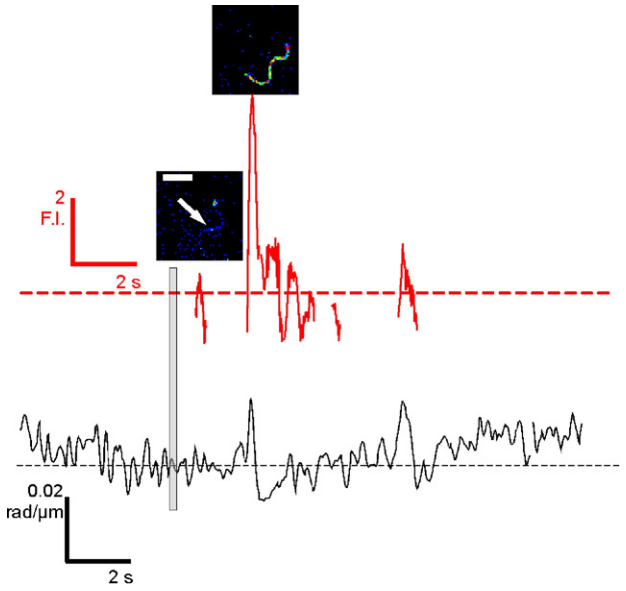

Fig. 4. Small increases in $[Ca^{2+}]_i$ that do not induce turns may precede larger increases in $[Ca^{2+}]_i$ at low concentrations of caged speract (1 nM). Red trace shows fluo-4 fluorescence in flagellum (average along length), with individual images (above the trace) extracted from complete image sequence. Scale bar = 20 μm. White arrow in first image indicates position of flagellum. Dashed line shows fluorescence intensity (FI) of 4. Black trace shows curvature of sperm trajectory derived from position of sperm head in each image, dashed line shows curvature of 0.05 rad/μm. Grey box indicates UV exposure (250 ms).

or with in addition 10 μM niflumic acid (lower panels). Beneath each image is the orientation of the flagellum normalised to a fixed head position. In sperm treated with caged speract alone, uncaging of speract induces a rapid rise in flagellar $[Ca^{2+}]_i$ which is accompanied by an transient (<100 ms) increase in flagellar asymmetry (asymmetric flagella shown in red). In the presence of 10 μM niflumic acid, the increase in flagellar $[Ca^{2+}]_i$ is greater and more prolonged (note that each image is extracted every 50 ms), as is the increase in flagellar asymmetry (red traces). In Fig. 5B the flagellum remains in a relatively asymmetric conformation until 725 ms after flagellar $[Ca^{2+}]_i$ begins to rise, an approximate 10-fold increase over non niflumic acid-treated sperm (see Movie 4 in supplementary material; see Supplementary Fig. 1 for the complete sequence of images for the niflumic acid-treated sperm shown in Fig. 5B). Fig. 5C shows the trajectory of a sperm treated with 20 μM niflumic acid, with the red trace indicating the path of the sperm during the speract-induced $[Ca^{2+}]_i$ fluctuations. Illustrated alongside is an extract showing the extended nature of the sperm turn during a single Ca^{2+} fluctuation. These extended turns were also inhibited by agents known to inhibit Ca_v channels; Fig. 3C shows that for sperm treated with 5 μM niflumic acid (grey trace), 200 μM Ni^{2+} was capable of markedly reducing the size and duration of sperm turns (black trace). These results together show that altering the characteristics of the phasic increase in flagellar Ca^{2+} by treating the sperm with niflumic acid profoundly alters the nature of the motility changes they produce, inasmuch as the turning events are no longer relatively transient, but are greatly prolonged.

Dose–response of effect of niflumic acid on Ca^{2+} fluctuations and sperm turns

We characterised the effect of varying concentrations of niflumic acid on the Ca^{2+} fluctuations, and how these in turn alter the motility parameters of the sperm trajectory. We analysed individual Ca^{2+} fluctuations according to the following 5 criteria: amplitude (F_p/F_b where F_p is the peak fluorescence intensity of fluo-4 in the flagella for each fluctuation, and F_b is the initial fluorescence intensity of fluo-4 in the flagella at the start of each fluctuation); $t_{1/2}$ increase; $t_{1/2}$ decrease; peak width at half-height; and interval between successive peaks. The results are presented in Fig. 6A. The Ca^{2+} fluctuations of sperm in the medium containing 1 μM niflumic acid were indistinguishable from those of control sperm recorded in medium containing 100 nM caged speract alone. In the presence of 5, 10 and 20 μM niflumic acid, all of the 5 characterising criteria increased in value, with the amplitude of the Ca^{2+} increase reaching a peak at 5 μM niflumic acid, and values for $t_{1/2}$ increase, $t_{1/2}$ decrease, peak width and peak interval reaching a maximum at 20 μM niflumic acid. Of the 182 Ca^{2+} peaks measured under all conditions, 172 were associated with spikes, or turning events, as shown by the measurements of the curvature of the sperm head trajectory (see Materials and methods for details of correlation procedure). These peaks in the sperm trajectory curvature were analysed using the parameters described for the $[Ca^{2+}]_i$ fluctuations and the results presented in Fig. 6B. As with the Ca^{2+} fluctuations, the trajectories of sperm in 1 μM niflumic acid were indistinguishable from control cells stimulated in the presence of 100 nM caged speract alone. Elevating the niflumic acid concentration also increased all the peak parameters in the curvature of the sperm trajectory, reaching a maximum at 20 μM niflumic acid. We next paired each Ca^{2+} fluctuation with its corresponding peak in the curvature (see Materials and methods for alignment criteria), and measured the correlation coefficients for each of the 4 criteria that describe the form of the peaks. All four were positively correlated, with the strongest relationship observed between peak widths. Niflumic acid treatment at 5–20 μM significantly decreased the frequency of fluctuations in flagellar $[Ca^{2+}]_i$ from an average inter-peak interval of 675 ms for sperm treated with 100 nM caged speract alone, to between 1075 and 1250 ms (Fig. 6B, graph 5). There were no statistically significant differences among the intervals between Ca^{2+} fluctuations within any of the conditions tested (data not shown).

In Fig. 7A, we compare the degree to which flagellar bending varies in individual flagella throughout the course of an experiment under differing conditions. After uncaging of 100 nM speract, or in the additional presence of 1 μM niflumic acid, sperm flagella bending varies within the quadrant below the long axis of the head that lies behind the head. At 5 μM niflumic acid the degree of flagellar bending increases, such that in numerous images the flagellum 'enters' the quadrant that lies below and in front of the head. Raising the niflumic acid concentration to 10 and 20 μM increases the bending further,

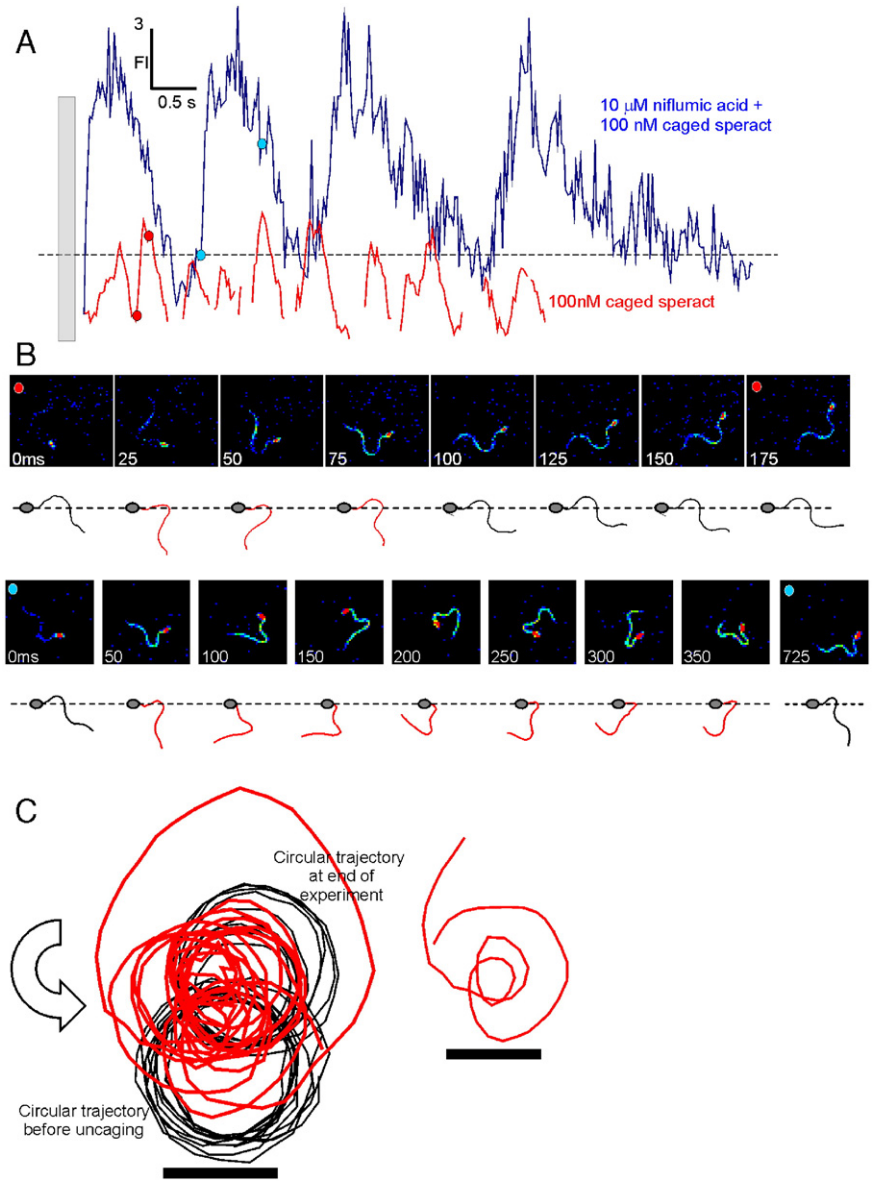

Fig. 5. Niflumic acid increases the duration, amplitude and interval between successive Ca^{2+} fluctuations. (A) Fluo-4 fluorescence in flagellum (average along length) of sperm exposed to 100 nM caged speract (red trace) or 100 nM caged speract and 10 μM niflumic acid (blue trace). Dashed line shows fluorescence intensity (FI) of 5. Grey box indicates UV exposure (250 ms). (B) Upper panel shows sequential images of sperm undergoing a single Ca^{2+} fluctuation extracted from sequence shown with red dots in red trace (100 nM caged speract) in panel A. Bottom panel of images are sequential images of sperm undergoing single Ca^{2+} fluctuation extracted from a sequence shown with blue dots in blue trace (100 nM caged speract+10 μM niflumic acid) in panel A. Beneath each image the position of the flagellum is shown normalised to a fixed head position. Red flagella have a greatly increased degree of bending. (C) Sperm swimming trajectory throughout experiment. The red line is the sperm trajectory during the phase of Ca^{2+} fluctuations, and black lines are the sperm trajectory outside the phase of Ca^{2+} fluctuations. Arrow indicates direction of circular swimming pathway. Scale bar=20 μm. Right shows extract from complete trajectory that shows the sperm trajectory during an individual Ca^{2+} fluctuation.

with the range spanning the almost the entire 180° arc below the sperm head. In Fig. 7B we incorporate the fluorescence intensity of the fluo-4 Ca^{2+} dye at each time point, whereby the area of the bubble represents the fluorescence intensity of the flagellum. The speract-treated sperm (red circles) shows that circles of different sizes are distributed relatively homogeneously throughout the range of flagellum asymmetries, indicating a poor correlation between flagellar $[Ca^{2+}]_i$ and the degree of bending. In contrast, in the presence of 10 μM niflumic acid (blue circles), only larger circles are found at the highest flagellar asymmetries, suggesting that a high flagellar $[Ca^{2+}]_i$ is necessary to achieve such extreme conformations. This conclusion is supported by correlating the clockwise angular displacement from the ordinate axis (a measure of the degree of flagellar bending) to the fluorescence intensity of the flagellum at each point in individual sperm. In sperm exposed to 100 nM caged speract alone, or in 1 μM niflumic acid, there is little or no correlation between these two variables in individual sperm (Fig. 7B, lower panel). In 5 μM niflumic acid, the correlation between fluorescence intensity and degree of asymmetry increases to between 0.23 and 0.54, a trend which is maintained at 10 and 20 μM niflumic acid. The positive

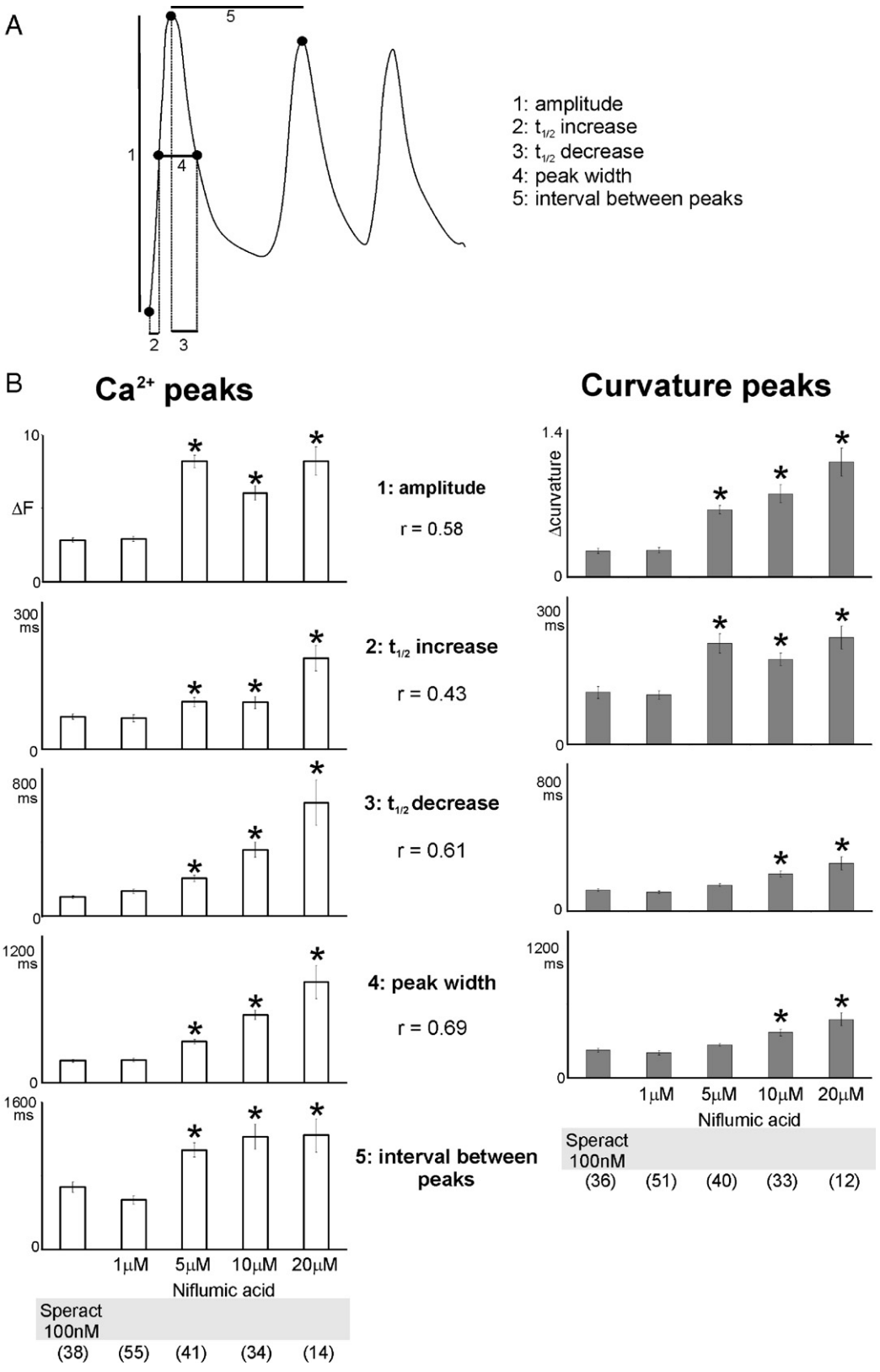

Fig. 6. Peak analysis of the fluctuations in $[Ca^{2+}]_i$ and curvature of the sperm trajectory. (A) The five criteria used to analyse (i) the fluctuations in $[Ca^{2+}]_i$ and (ii) the peaks in the curvature of the sperm trajectory. (B) Left column of bar charts shows effect of increasing concentration of niflumic acid on the five criteria in panel A as applied to fluctuations in $[Ca^{2+}]_i$. Right column of bar charts shows the effect of increasing concentration of niflumic acid on the four criteria related to peak kinetics as outlined in panel A. *r* is the Pearson correlation coefficient between temporally aligned peaks in $[Ca^{2+}]_i$ and curvature of trajectory as defined by the four criteria related to peak kinetics. Numbers in parenthesis indicate number of peaks analysed. Asterisks denote statistically significant difference (ANOVA) to sperm treated with 100 nM caged speract alone. Error bars show S.E.M.

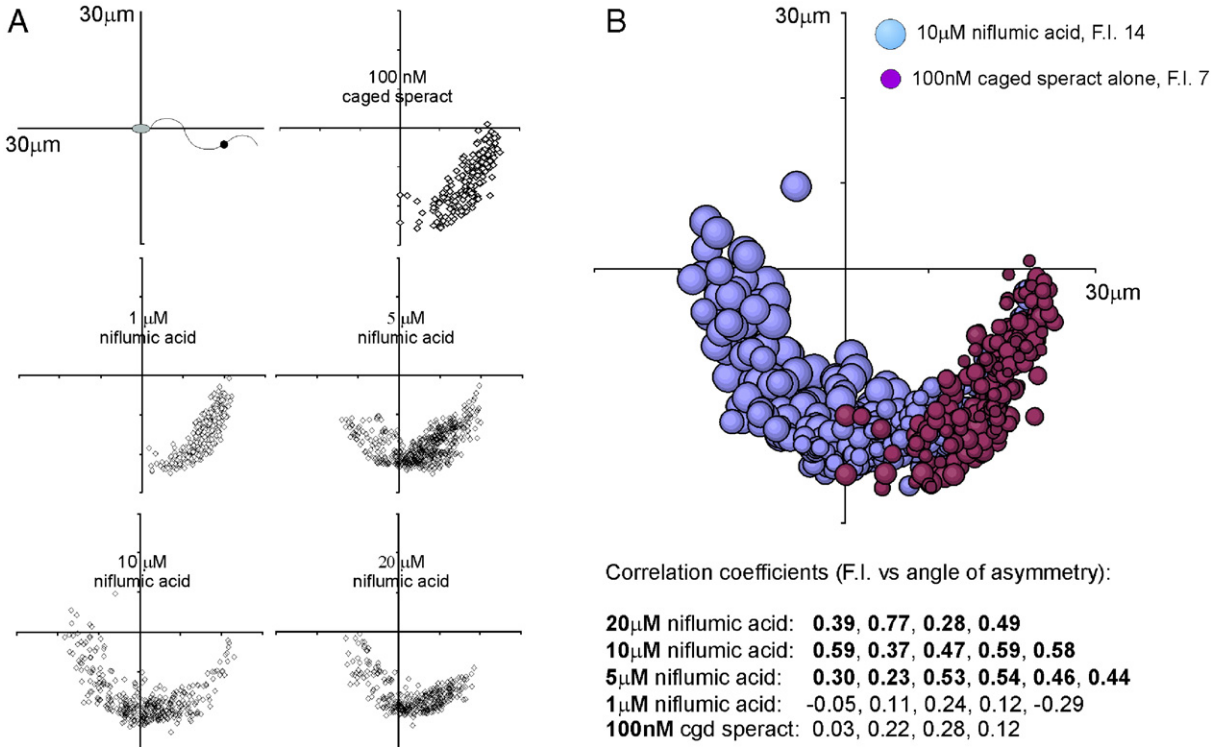

Fig. 7. Niflumic acid enhances the increase in flagellar bending produced by speract. (A) Upper left panel shows how an arbitrarily chosen point 28 μm along the sperm flagellum is plotted in each frame of each experimental condition. Position of head normalised to the origin in every frame. Remaining panels show how the position and the degree of bending of flagellum varies throughout complete experiment in sperm treated with 100 nM caged speract alone (upper right), or in the additional presence of 1–20 μM niflumic acid. (B) Comparison of the position of flagellum to its fluorescence intensity as depicted by size of circle. Red circles – sperm treated with 100 nM caged speract. Blue circles – sperm treated with 100 nM caged speract and 10 μM niflumic acid. Numbers below graph show the Spearman rank correlation coefficients for comparison between FI and the degree of asymmetry for individual sperm treated as indicated. Numbers in bold type indicate a statistically significant monotonic increase ($p < 0.001$).

correlation between flagellar bending and $[Ca^{2+}]_i$ is statistically significant for experiments performed in 5–20 μM niflumic acid. In the absence of niflumic acid or at 1 μM niflumic acid, no statistically significant positive correlation was observed, despite the fact that in two experiments the calculated positive correlation (0.24 and 0.28) was greater than or equal to two of the correlations (0.23 and 0.28) calculated at higher niflumic acid concentrations. This is because at 5 μM niflumic acid and above the increases in $[Ca^{2+}]_i$ in the flagellum are prolonged, leading to an increased sample number over the course of an experiment.

Collectively these data suggest that in the presence of niflumic acid the relationship between $[Ca^{2+}]_i$ and flagellar asymmetry is at least partly proportional, although it is clear from Fig. 5B that the flagella still return to a more symmetric conformation while $[Ca^{2+}]_i$ remains relatively elevated.

Niflumic acid increases and extends the E_m depolarisation following speract addition

The best known targets of niflumic acid are CaCC, and thus understanding its effects on sperm membrane potential (E_m) requires knowing the Cl^- equilibrium potential (E_{Cl}). We calculated the resting intracellular Cl^- concentration ($[Cl^-]_i$) using the null point technique (see Materials and methods). Changes in pH_i upon addition of the Cl^-/OH^- exchanger tributyl tin were recorded using the pH-sensitive dye BCECF in varying concentrations of external Cl^- ($[Cl^-]_e$). An example of a sequence of pH changes under these conditions is presented in Fig. 8A. The average $[Cl^-]_i$ was 31.7±8.5 mM ($n=6$), which we used to derive the E_{Cl} as follows:

$$E_{Cl} = (RT/F)\ln([Cl^-]_i/[Cl^-]_e) = -68.5 \text{ mV}$$

(between −62.6 mV and −76.2 mV) at 15 °C, assuming $[Cl^-]_e$ is 500 mM and where the value for RT/F was obtained from Hille (1992).

Given that the resting potential of *S. purpuratus* sperm is ~−40 mV (Gonzalez-Martínez and Darszon, 1987; Schackmann et al., 1981), opening of Cl^- channels would result in an influx of Cl^- ions and hyperpolarisation of the sperm.

We then examined whether inhibiting CaCC with niflumic acid altered speract-induced E_m changes. Using the slow-response membrane potential dye $DiSC_3$ we measured the changes to E_m upon exposure to 100 nM speract, and in the additional presence of 1, 5 or 20 μM niflumic acid. As reported previously, speract induces a hyperpolarisation followed by an E_m depolarisation in sperm populations (Beltran et al., 1996; Darszon et al., 2006; Labarca et al., 1996; Lee and Garbers, 1986). In the presence of 20 μM niflumic acid there is a small,

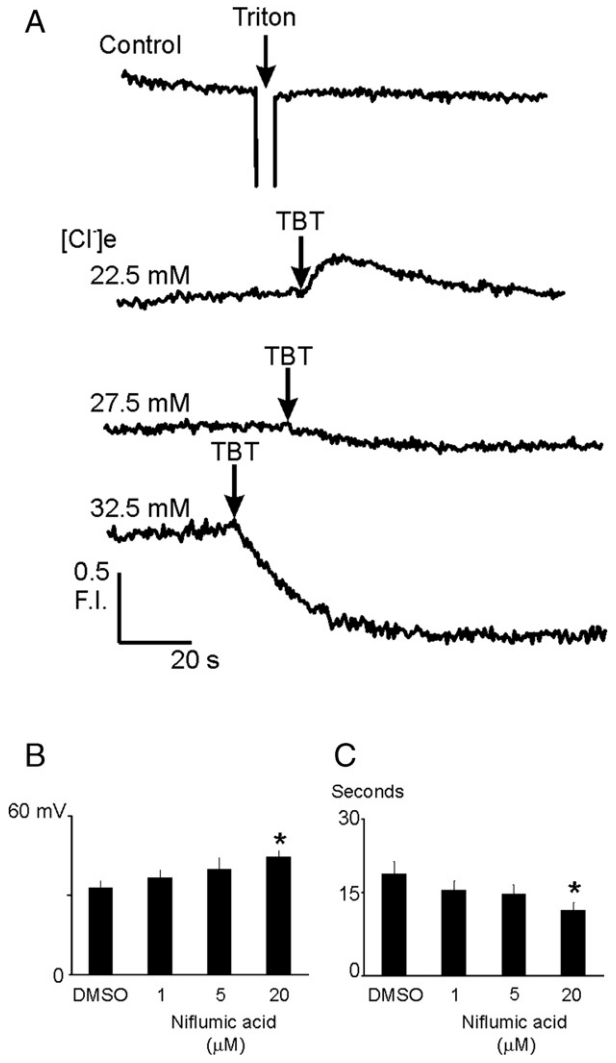

Fig. 8. Niflumic acid enhances the speract-induced Em depolarisation and reduces the time-to-peak depolarisation. (A) Null-point determination of $[Cl^-]_i$ by recording changes in pH_i (measured with fluorescent indicator BCECF). Upper trace: release of BCECF from cells suspended in media indicated in Materials and methods by addition of 0.025% Triton X-100 does not result in a large fluorescence change, indicating that external and internal pH is closely matched. Lower three traces show change in pH_i upon addition of tributyltin (Cl^-/OH^- exchanger) in sperm from one urchin in ASW containing the indicated $[Cl^-]_e$. Average result from six animals presented in text. Scale is arbitrary (fluorescence intensity (FI)). (B) Effect of niflumic acid on the size of the Em depolarisation induced by 100 nM speract ($n=5$). Error bars represent S.E.M., asterisk indicates statistically significant difference to control. (C) Effect of niflumic acid on the time-to-peak depolarisation induced by 100 nM speract ($n=5$). Error bars represent S.E.M.; asterisk indicates statistically significant difference to control.

but statistically significant, increase in amplitude (Fig. 8B) and decrease in the time-to-peak (Fig. 8C).

Discussion

We have examined the effect of speract, a decapeptide component of the egg investments of *S. purpuratus*, on both $[Ca^{2+}]_i$ and sperm motility by simultaneously measuring fluo-4 fluorescence and flagellar form in motile sperm. We found that speract triggers a train of transient Ca^{2+} increases, and that associated with nearly every fluctuation was a sharp and transient increase in flagellar bending, which led the sperm to undergo a turn. Each turn was most commonly superimposed on a background trajectory of decreased curvature, such that the sperm performed a series of turns interspersed with periods of straighter swimming. This pattern of motility is seen in sperm of many marine species undergoing chemotaxis (e.g. Yoshida et al., 2003), including *A. punctulata*, and has been termed the 'turn-and-run' model (Bohmer et al., 2005). We also report a subset of sperm that produce the same series of turns, but superimposed on a tonic increase in the curvature of the trajectory. The swimming behaviour of this proportionately smaller sperm population resembles that seen in sperm exposed to relatively high concentrations of caged speract (Shiba et al., 2005).

The mechanism underlying the difference between the two populations is unknown, but appears to be independent of phasic Ca^{2+} fluctuations, and also under dynamic control as we observed a sperm migrate rapidly from the majority to the minority population during the course of a single experiment. Translating the circular motion of the sperm into a three-dimensional helix, the sperm exhibiting the turn-and-run response would deviate significantly from the original path of the helix, thus causing the sperm to traverse a greater volume of sea water in its search for the egg. In contrast, sperm that swim in smaller circles in response to speract will swim in a straighter and narrower helix in vivo, which may represent another strategy altogether, or the second phase of a dual strategy, to improve the probability of sperm–egg encounter. We have called these two phases of motility response to speract the 'search' and the 'sprint' stages, and more work is required to understand the mechanism regulating the switch between each phase, and what the purpose of each stage might be.

The mechanism of SAP signalling in sperm is yet to be fully characterised. Current models are based upon an initial activation of guanylate cyclase leading to an increase in cGMP which in turn hyperpolarizes sperm most likely by opening of cGMP-gated K^+ channels (Darszon et al., 2001, 2005; Galindo et al., 2007; Strunker et al., 2006). It is further proposed that this hyperpolarisation removes inactivation from Ca_v channels which subsequently open following depolarisation, which in turn produces the rapid, transient increases in $[Ca^{2+}]_i$ that induce transient increases in flagellar bending (Babcock et al., 1992; Bohmer et al., 2005; Kaupp et al., 2003; Wood et al., 2003). Previous studies have shown that more than one Ca^{2+} entry pathway exists in sea urchin sperm flagella, and that it is the opening of the putative Ca_v-channel-mediated 'fast' pathway that is required to generate turns (Wood et al., 2005). Activation of a slower route of Ca^{2+} entry that is present in the head and flagella, possibly mediated by cAMP increases, does not appear to influence sperm turns (Cook and Babcock, 1993a; Kaupp et al., 2003; Wood et al., 2003, 2005). It is thus interesting to note that at low concentrations of caged speract, we occasionally observed a small, transient increase in flagellar Ca^{2+} that did not measurably influence flagellar

asymmetry. One possible explanation is that a threshold number of Ca_v channels are required to open before the increase in asymmetry is triggered and, at low concentrations, speract induces a weak hyperpolarisation sufficient to remove inactivation from only a subset of Ca_v channels. This would be more probable if a mixed population of Ca_v channels is present in sea urchin sperm, as seems likely for both *S. purpuratus* and *A. punctulata* (Granados-Gonzalez et al., 2005; Strunker et al., 2006).

The sensitivity of both cGMP- (Wood et al., 2005) and speract-stimulated Ca^{2+} increases in the flagella to blockade by nimodipine and Ni^{2+} suggests that they activate the same Ca^{2+} entry pathway, although we do not know why release of caged cGMP induces a single Ca^{2+} fluctuation, and not the train of Ca^{2+} fluctuations induced by speract. It is feasible that the cGMP-uncaging experiments liberate cGMP concentrations much greater than those reached after speract exposure, and/or that the spatial compartmentalisation of cGMP increases is important in generating fluctuations.

We next investigated whether altering the characteristics of the Ca^{2+} fluctuations affected the sperm motility. In immobilised *S. purpuratus* sperm niflumic acid enhances the duration and amplitude of phasic Ca^{2+} fluctuations, and increases the inter-peak interval (Wood et al., 2003). We confirmed that the same effect occurs in motile cells. We further show that the change in flagellar bending mirrors the altered kinetics of the increase in $[Ca^{2+}]_i$, with a positive correlation observed between various parameters used to compare the peaks in $[Ca^{2+}]_i$ and the curvature of the sperm trajectory. This demonstrates that the fast Ca^{2+} entry pathway is not only necessary to generate sperm turns, but that the kinetics of this Ca^{2+} entry are important in determining the nature of these turns. Thus the alterations to flagellar form that underpin each turn are not fixed sequences of events that are triggered once by each permissive Ca^{2+} entry event, but may be shaped and modified by the kinetics of the increase in $[Ca^{2+}]_i$. The importance of this point is demonstrated by the sperm trajectories shown in Figs. 1 and 5. Only the combination of sperm turns superimposed on a background of straighter swimming reproduced the typical motility patterns seen in chemotactic sea urchin sperm; if the 'straighter swimming' component was absent (Fig. 1B) or if the turns were greatly extended in duration (Fig. 5), the sperm no longer relocated its swimming trajectory over a larger area. This may be relevant to the fine directional control of motility observed during chemotaxis in other model systems.

The sensitivity to niflumic acid suggests that CaCC are present in sea urchin sperm and play a role in motility. Cl^- channel activity sensitive to DIDS, another anion transport and channel inhibitor, has been reported in planar bilayers containing a wheat germ agglutinin Sepharose column-enriched detergent-solubilized protein fraction from sperm plasma membranes (Morales et al., 1993). Also, anion channels sensitive to blockade by niflumic acid have been characterised from mammalian sperm (Espinosa et al., 1998), and CaCC-mediated Cl^- currents have been found in cilia of olfactory receptor neurons that are inhibited by niflumic acid (Kleene and Gesteland, 1991; Madrid et al., 2005). How might such channels participate in the speract signalling pathway? If CaCC channels are present, they would open in response to Ca^{2+} entry, leading to influx of Cl^- ions and E_m hyperpolarisation. This hyperpolarisation could (1) reverse Ca^{2+} influx by activating a Na^+/Ca^{2+} exchange activity to extrude Ca^{2+} from the cell, thus shaping the $[Ca^{2+}]_i$ increase into a transient fluctuation; and (2) open hyperpolarisation-activated and cyclic nucleotide-gated (HCN) channels (Galindo et al., 2005; Gauss et al., 1998), depolarising the cell, opening Ca_v channels and setting up a cycle of Ca^{2+} influx and efflux through the concerted action of HCN, Ca_v and CaCC channels (Fig. 9). This model explains how

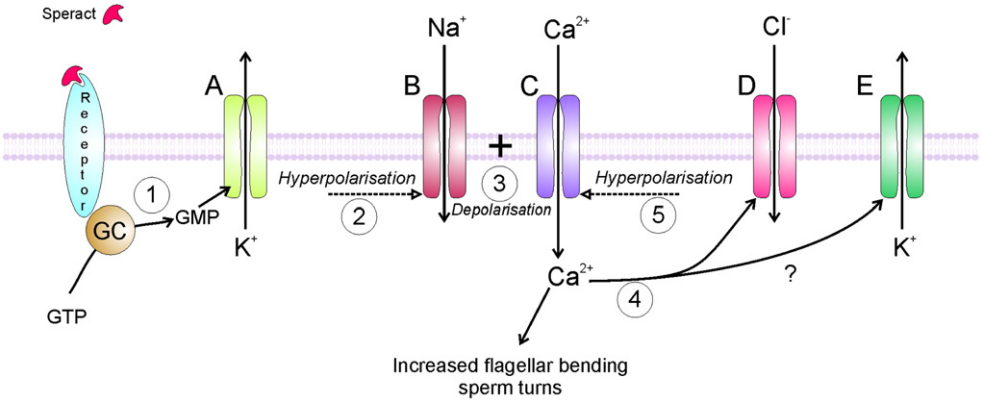

Fig. 9. A model for the concerted action of ion channels and ion flux in the generation of repetitive, transient Ca^{2+} fluctuations in sea urchin sperm flagella. Speract binds to its receptor, activating a guanylate cyclase activity (GC). (1) The increased levels of cGMP directly activate a K^+ channel (A), possibly Sp-tetraKCNG, leading to hyperpolarisation of the membrane potential. (2) The hyperpolarisation activates spHCN channels (B) and removes inactivation from Ca_v channels (C). (3) The membrane potential repolarises, opening Ca_v channels, and increases in intracellular Ca^{2+} and Na^+ lead to further depolarisation. The increase in Ca^{2+} levels in the flagellum enhances flagellar bending and leads the sperm to turn via an unknown mechanism operating in the axoneme. (4) Increased Ca^{2+} levels open CaCC (D). We do not discard the possibility that Ca^{2+}-sensitive K^+ channels (E) are present in the flagellum and may also open at this point. (5) Cl^- influx, with a possible contribution from K^+ efflux, hyperpolarises the membrane potential, removing inactivation from Ca_v channels and opening spHCN channels. The hyperpolarisation will also activate Na^+/Ca^{2+} exchangers that remove Ca^{2+} from the cytosol (not shown). Stages 4 and 5 are then cyclically repeated to generate a train of Ca^{2+} increases that produce a repetitive sequence of sperm turns. The sequence continues until one or more of the molecular components in the pathway are downregulated.

sperm might generate trains of Ca^{2+} fluctuations lasting >20 s after the initial exposure to speract, based on the assumption that a hyperpolarisation–depolarisation cycle generates each fluctuation. The initial, cGMP-gated K^+ channel-generated hyperpolarisation that most likely triggers the first Ca^{2+} fluctuation is unlikely to alone generate all of the subsequent hyperpolarisation–depolarisation cycles, as guanylate cyclase activity declines rapidly (within 5 s) after initial SAP exposure (Bentley et al., 1986; Suzuki et al., 1984; Ward and Vacquier, 1983), as do cGMP levels (Kaupp et al., 2003; Shimomura and Garbers, 1986). Thus additional mechanisms must be in place to generate the trains of Ca^{2+} fluctuations that last up to 20 s or more, in which we propose CaCC channels play an important role.

In the presence of the CaCC inhibitor niflumic acid the depolarisation phase of the cycle would be prolonged, leading to increased amplitude and duration of Ca^{2+} influx. Interestingly, niflumic acid has also been shown to inhibit HCN channels, whose activation voltage is shifted to a more negative potential in amphibian photoreceptors and mammalian heart pacemaker cells (Accili and DiFrancesco, 1996; Satoh and Yamada, 2001). This increases the delay between successive pacemaker-regulated events, such as we observe in the case of the delay between successive Ca^{2+} fluctuations in sea urchin sperm. This proposed model also explains our observation that the degree of flagellar bending and the $[Ca^{2+}]_i$ are more positively correlated in the presence of 5–20 μM niflumic acid. In the absence of niflumic acid, Ca_v channel opening is normally a relatively transient event due to Ca^{2+}-stimulated activation of CaCC leading to E_m hyperpolarisation and closure of Ca_v channels. Other channels, such as K^+ channels, could contribute to this hyperpolarisation. Thus the flagella rapidly revert back to a more symmetric form, while Ca^{2+} levels fall after a short lag, and it is this lag that manifests as a lack of proportionality between the two factors. In the presence of niflumic acid, Ca^{2+} entry is increased and prolonged, and the degree of flagellar bending is simultaneously increased and prolonged, such that an analysis of the correlation between the two factors is reasonably positive.

It is interesting to note that the speract-induced motility changes in *S. purpuratus* sperm closely resemble those of other marine species whose sperm undergo chemotaxis (e.g. the turn-and-run model proposed for *A. punctulata*), and yet speract is not a chemoattractant, at least with *S. purpuratus* sperm. Therefore the motility pattern of turns interspersed with periods of straighter swimming must be considered necessary but not sufficient for chemotaxis. The difference in the SAP signalling mechanisms of these two species that accounts for the divergence in motility pattern is unknown, but it is possible that the subtle manipulations of the kinetics of Ca^{2+} entry that determine the duration and acuteness of sperm turns serves to 'fine tune' the direction of sperm swimming during chemotaxis. Part of the answer for why two such similar yet differing strategies for enhancing reproductive success evolved must lie in the natural environment in which differing marine organisms live and reproduce. We are currently examining such factors as a means to understand this divergence.

Acknowledgments

The authors would like to thank Gabriel Gasque for programming the peak analysis functions in Igor Pro. The work was supported by CONACyT, DGAPA (UNAM) and The Wellcome Trust.

Appendix A. Supplementary data

Supplementary data associated with this article can be found, in the online version, atdoi:10.1016/j.ydbio.2007.03.036.

References

Accili, E.A., DiFrancesco, D., 1996. Inhibition of the hyperpolarization-activated current (if) of rabbit SA node myocytes by niflumic acid. Pflugers Arch. 431, 757–762.

Baba, S.A., Mogami, Y., 1985. An approach to digital image analysis of bending shapes of eukaryotic flagella and cilia. Cell Motil. 5, 475–489.

Babcock, D.F., 1983. Examination of the intracellular ionic environment and of ionophore action by null point measurements employing the fluorescein chromophore. J. Biol. Chem. 258, 6380–6389.

Babcock, D.F., et al., 1992. Early persistent activation of sperm K^+ channels by the egg peptide speract. Proc. Natl. Acad. Sci. U. S. A. 89, 6001–6005.

Beltran, C., et al., 1996. Membrane potential regulates sea urchin sperm adenylylcyclase. Biochemistry 35, 7591–7598.

Bentley, J.K., et al., 1986. Receptor-mediated activation of spermatozoan guanylate cyclase. J. Biol. Chem. 261, 14859–14862.

Bohmer, M., et al., 2005. Ca^{2+} spikes in the flagellum control chemotactic behavior of sperm. EMBO J. 24, 2741–2752.

Brokaw, C.J., 1974. Calcium and flagellar response during the chemotaxis of bracken spermatozoids. J. Cell. Physiol. 83, 151–158.

Cardullo, R.A., et al., 1994. Speract receptors are localized on sea urchin sperm flagella using a fluorescent peptide analog. Dev. Biol. 162, 600–607.

Cook, S.P., Babcock, D.F., 1993a. Activation of Ca^{2+} permeability by cAMP is coordinated through the pH_i increase induced by speract. J. Biol. Chem. 268, 22408–22413.

Cook, S.P., Babcock, D.F., 1993b. Selective modulation by cGMP of the K^+ channel activated by speract. J. Biol. Chem. 268, 22402–22407.

Cook, S.P., et al., 1994. Sperm chemotaxis: egg peptides control cytosolic calcium to regulate flagellar responses. Dev. Biol. 165, 10–19.

Cosson, M.P., et al., 1984. Sperm chemotaxis in siphonophores: II. Calcium-dependent asymmetrical movement of spermatozoa induced by the attractant. J. Cell Sci. 68, 163–181.

Cosson, J., et al., 2003. How spermatozoa come to be confined to surfaces. Cell Motil. Cytoskelet. 54, 56–63.

Dangott, L.J., Garbers, D.L., 1984. Identification and partial characterization of the receptor for speract. J. Biol. Chem. 259, 13712–13716.

Darszon, A., et al., 2001. Ion transport in sperm signaling. Dev. Biol. 240, 1–14.

Darszon, A., et al., 2005. Calcium channels and Ca^{2+} fluctuations in sperm physiology. Int. Rev. Cytol. 243, 79–172.

Darszon, A., et al., 2006. Sperm channel diversity and functional multiplicity. Reproduction 131, 977–988.

Eisenbach, M., Giojalas, L.C., 2006. Sperm guidance in mammals – an unpaved road to the egg. Nat. Rev., Mol. Cell Biol. 7, 276–285.

Espinosa, F., et al., 1998. Mouse sperm patch-clamp recordings reveal single Cl^- channels sensitive to niflumic acid, a blocker of the sperm acrosome reaction. FEBS Lett. 426, 47–51.

Galindo, B.E., et al., 2000. Participation of a K(+) channel modulated directly by cGMP in the speract-induced signaling cascade of *Strongylocentrotus purpuratus* sea urchin sperm. Dev. Biol. 221, 285–294.

Galindo, B.E., et al., 2005. A new hyperpolarization-activated, cyclic nucleotide-gated channel from sea urchin sperm flagella. Biochem. Biophys. Res. Commun. 334, 96–101.

Galindo, B.E., et al., 2007. Sp-tetraKCNG: a novel cyclic nucleotide gated K(+) channel. Biochem. Biophys. Res. Commun. 354, 668–675.

Garbers, D.L., 1989. Molecular basis of fertilization. Annu. Rev. Biochem. 58, 719–742.

Gauss, R., et al., 1998. Molecular identification of a hyperpolarization-activated channel in sea urchin sperm. Nature 393, 583–587.

Gonzalez-Martínez, M., Darszon, A., 1987. A fast transient hyperpolarization occurs during the sea urchin sperm acrosome reaction induced by egg jelly. FEBS Lett. 218, 247–250.

Granados-Gonzalez, G., et al., 2005. Identification of voltage-dependent Ca^{2+} channels in sea urchin sperm. FEBS Lett. 579, 6667–6672.

Hansbrough, J.R., Garbers, D.L., 1981. Speract. Purification and characterization of a peptide associated with eggs that activates spermatozoa. J. Biol. Chem. 256, 1447–1452.

Harumi, T., et al., 1992. Effects of sperm-activating peptide on *Hemicentrotus pulcherrimus* spermatozoa in high potassium sea water. Dev. Growth Differ. 34, 163–172.

Hille, B., 1992. Ionic Channels of Excitable Membranes. Sinauer Associates, Sunderland, MA.

Kaupp, U.B., et al., 2003. The signal flow and motor response controlling chemotaxis of sea urchin sperm. Nat. Cell Biol. 5, 109–117.

Kaupp, U.B., et al., 2006. Sperm chemotaxis in marine invertebrates – molecules and mechanisms. J. Cell Physiol. 208, 487–494.

Kleene, S.J., Gesteland, R.C., 1991. Calcium-activated chloride conductance in frog olfactory cilia. J. Neurosci. 11, 3624–3629.

Labarca, P., et al., 1996. A cAMP regulated K^+-selective channel from the sea urchin sperm plasma membrane. Dev. Biol. 174, 271–280.

Lee, H.C., Garbers, D.L., 1986. Modulation of the voltage-sensitive Na^+/H^+ exchange in sea urchin spermatozoa through membrane potential changes induced by the egg peptide speract. J. Biol. Chem. 261, 16026–16032.

Madrid, R., et al., 2005. Cyclic AMP cascade mediates the inhibitory odor response of isolated toad olfactory receptor neurons. J. Neurophysiol. 94, 1781–1788.

Miller, R.L., Brokaw, C.J., 1970. Chemotactic turning behaviour of *Tubularia spermatozoa*. J. Exp. Biol. 52, 699–706.

Miller, R., 1985. Sperm chemo-orientation in the metazoa. In: Metz, C., Monroy, A. (Eds.), Biology of Fertilization. Academic Press, New York, pp. 275–337.

Morales, E., et al., 1993. Anion channels in the sea urchin sperm plasma membrane. Mol. Reprod. Dev. 36, 174–182.

Nishigaki, T., et al., 2004. A sea urchin egg jelly peptide induces a cGMP-mediated decrease in sperm intracellular Ca(2+) before its increase. Dev. Biol. 272, 376–388.

Pacaud, P., et al., 1989. Calcium-activated chloride current in rat vascular smooth muscle cells in short-term primary culture. Pflugers Arch. 413, 629–636.

Ramarao, C.S., Garbers, D.L., 1985. Receptor-mediated regulation of guanylate cyclase activity in spermatozoa. J. Biol. Chem. 260, 8390–8396.

Reynaud, E., et al., 1993. Ionic bases of the membrane potential and intracellular pH changes induced by speract in swollen sea urchin sperm. FEBS Lett. 329, 210–214.

Rodriguez, E., Darszon, A., 2003. Intracellular sodium changes during the speract response and the acrosome reaction in sea urchin sperm. J. Physiol. 546, 89–100.

Satoh, T.O., Yamada, M., 2001. Niflumic acid reduces the hyperpolarization-activated current (I(h)) in rod photoreceptor cells. Neurosci. Res. 40, 375–381.

Schackmann, R.W., Chock, P.B., 1986. Alteration of intracellular [Ca^{2+}] in sea urchin sperm by the egg peptide speract. Evidence that increased intracellular Ca^{2+} is coupled to Na^+ entry and increased intracellular pH. J. Biol. Chem. 261, 8719–8728.

Schackmann, R.W., et al., 1981. Membrane potential depolarization and increased intracellular pH accompany the acrosome reaction of sea urchin sperm. Proc. Natl. Acad. Sci. U. S. A. 78, 6066–6070.

Shiba, K., et al., 2005. Sperm-activating peptide induces asymmetric flagellar bending in sea urchin sperm. Zoolog. Sci. 22, 293–299.

Shimomura, H., Garbers, D.L., 1986. Differential effects of resact analogues on sperm respiration rates and cyclic nucleotide concentrations. Biochemistry 25, 3405–3410.

Spehr, M., et al., 2003. Identification of a testicular odorant receptor mediating human sperm chemotaxis. Science 299, 2054–2058.

Strunker, T., et al., 2006. A K(+)-selective cGMP-gated ion channel controls chemosensation of sperm. Nat. Cell Biol. 8, 1149–1154.

Suzuki, N., et al., 1984. A peptide associated with eggs causes a mobility shift in a major plasma membrane protein of spermatozoa. J. Biol. Chem. 259, 14874–14879.

Tatsu, Y., et al., 2002. A caged sperm-activating peptide that has a photocleavable protecting group on the backbone amide. FEBS Lett. 525, 20–24.

Ward, G.E., Vacquier, V.D., 1983. Dephosphorylation of a major sperm membrane protein is induced by egg jelly during sea urchin fertilization. Proc. Natl. Acad. Sci. U. S. A. 80, 5578–5582.

Ward, G.E., et al., 1985. Chemotaxis of *Arbacia punctulata* spermatozoa to resact, a peptide from the egg jelly layer. J. Cell Biol. 101, 2324–2329.

Wood, C.D., et al., 2003. Speract induces calcium oscillations in the sperm tail. J. Cell Biol. 161, 89–101.

Wood, C.D., et al., 2005. Real-time analysis of the role of Ca(2+) in flagellar movement and motility in single sea urchin sperm. J. Cell Biol. 169, 725–731.

Yoshida, M., et al., 2003. Store-operated calcium channel regulates the chemotactic behavior of ascidian sperm. Proc. Natl. Acad. Sci. U. S. A. 100, 149–154.